A dual triangular pyramidal indentation technique for material property evaluation

Minsoo Kim
Department of Mechanical Engineering, Sogang University, Seoul 121-742, Republic of Korea

Jin Haeng Lee
Research Reactor Mechanical Structure Design Division, Korea Atomic Energy Research Institute, Daejeon 305-353, Republic of Korea

Felix Rickhey and Hyungyil Lee[a)]
Department of Mechanical Engineering, Sogang University, Seoul 121-742, Republic of Korea

(Received 26 September 2014; accepted 12 February 2015)

In this study, a method using dual triangular pyramidal indenters is suggested for material property evaluation. First, we demonstrate that the load–depth curves and the projected contact areas from conical and triangular pyramidal indentations are generally different. Nonequal projected contact areas of two indenters and nonplanar contact line of Berkovich indenter are the main sources of different indentation characteristics of two indenters. For this reason, an independent approach to the triangular pyramidal indentation is needed. With finite element (FE) indentation analyses for various materials, we investigate the relationships between material properties, indentation parameters, and load–depth curves. Based on the FE solutions, we suggest mapping functions for evaluating material properties from indentations by two triangular pyramidal WC indenters, which differ in their centerline-to-face angles. Elastic modulus, yield strength, and strain hardening exponent are obtained with an average error of $<3\%$.

I. INTRODUCTION

Tensile and compression tests have long been used to obtain material properties. However, there are limitations in terms of specimen preparation and equipment when it comes to the application to micro/nano materials. On the other hand, by indentation tests, unlike tensile or compression tests, we can predict and measure material properties from load–depth curves by applying micro/nano indentation to micro/nano materials or the part in use. For these reasons, there have been many studies on instrumented indentation tests.[1–3]

The loading curves from self-similar indenters, e.g., conical and pyramidal indenters, generally follow Kick's law[4]:

$$P = C h_t^2 \quad , \tag{1}$$

where P, h_t, and C are indentation load, indentation depth, and Kick's law coefficient, respectively. To obtain material properties of a given material from an indentation test, there should be a one-to-one match between the load–depth curve obtained from an indentation test and its material properties. However, equal load–depth curves can be obtained for different materials due to the self-similarity of sharp indenters.[5,6] Previous studies[7,8] tried to solve this problem by using the concept of representative strain ε_R, which changes with the half-included angle of the indenter. Most of the reverse analysis methods are based on the concept of ε_R introduced by Tabor.[9] With Eq. (2), Dao et al.[7] found that stress–strain curves having the same C exhibit the same true stress at $\varepsilon_R = 0.033$ for sharp indentation.

$$\sigma_R = \sigma_0 \left(1 + \frac{E}{\sigma_0}\varepsilon_R\right)^n \quad . \tag{2}$$

Here σ_R is the representative stress, σ_0 is the yield strength, E is the Young's modulus, n is the strain hardening exponent. Based on Dao's[7] study, Cao and Lu[10] provided an analytical framework for extracting plastic properties of metals from the load–depth curve of spherical indentation. However, the definition of ε_R and values of ε_R themselves varied from study to study; It is hard to define the master σ_R and ε_R applicable to all kinds of materials. Lee et al.[11] showed that definitions of σ_R and ε_R in the literature depend partly on material properties, not only indenter angle for sharp indenter and indentation depth for spherical indenter. They even questioned the representativeness of ε_R. This motivates us to find a method for material property evaluation without adopting the concept of ε_R.

Contributing Editor: George M. Pharr
[a)]Address all correspondence to this author.
e-mail: hylee@sogang.ac.kr
DOI: 10.1557/jmr.2015.67

 © Materials Research Society 2015

https://doi.org/10.1557/jmr.2015.67 Published online by Cambridge University Press

Beghini et al.[12] determined the parameters of stress–strain relation from the inverse FE model in spherical indentation. Bobzin et al.[13] proposed a method to determine the plastic flow curve of thin coatings with spherical indenter. Using the method of Juliano,[14] they determined the yield stress based on the load–depth curve from nanoindentation. In contrast to a spherical indenter, a single sharp indenter[15,16] cannot provide mechanical properties. Lee et al.,[6] Cheng and Cheng,[17] and Swaddiwudhipong et al.[18] also showed that there are many materials with equal values of Kick's law coefficient C. To solve this

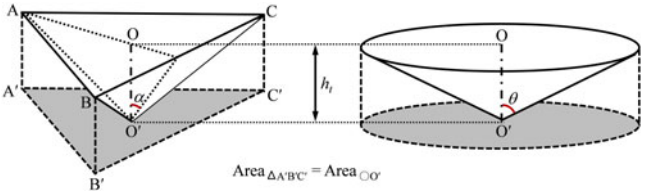


FIG. 1. Schematic diagram of a triangular pyramidal indenter with the indenter angle α, and its equivalent axisymmetric conical indenter with the indenter angle θ giving the same projected area.

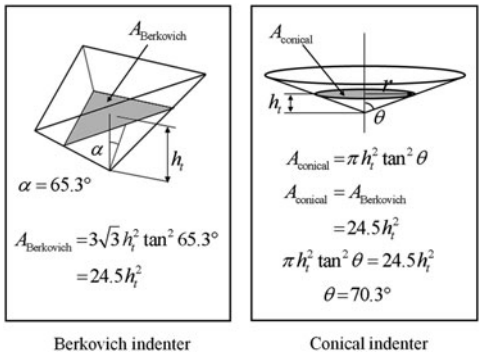


FIG. 2. Schematic of two indenters with the same projected contact area.

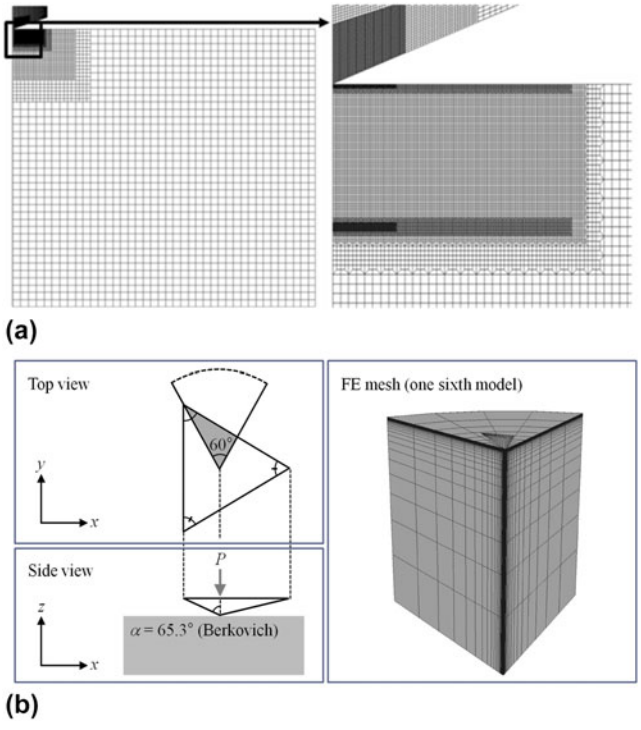


FIG. 3. Overall mesh design (a) using axisymmetric conical indenter and (b) 1/6 triangular pyramidal indenter (α = 65.3°; Berkovich).

TABLE I. Comparison of A and c^2 for two different indenters (E = 200 GPa, h_{max} = 0.05 mm).

		A ($\times 10^{-3}$ mm^2)			c^2		
ε_0	n	Berkovich (α = 65.3°)	Conical (θ = 70.3°)	Gap (%)	Berkovich (α = 65.3°)	Conical (θ = 70.3°)	Gap (%)
	2	49.03	47.15	4.0	0.894	0.880	1.5
	3	60.10	58.26	3.2	0.989	0.975	1.5
	5	70.32	68.10	3.3	1.070	1.052	1.8
0.001	7	73.36	72.47	1.2	1.093	1.084	0.9
	10	77.05	76.69	0.5	1.120	1.114	0.5
	13	80.14	79.88	0.3	1.142	1.136	0.5
	20	83.50	83.42	0.1	1.166	1.161	0.5
	2	46.05	44.73	3.0	0.866	0.858	0.9
	3	56.54	54.86	3.1	0.960	0.947	1.3
	5	66.25	63.04	5.1	1.039	1.013	2.5
0.002	7	70.68	67.38	4.9	1.073	1.046	2.6
	10	73.42	71.85	2.2	1.093	1.079	1.3
	13	75.68	73.71	2.7	1.110	1.093	1.6
	20	78.25	77.00	1.6	1.129	1.116	1.1
	2	45.88	43.24	6.1	0.864	0.844	2.4
	3	56.14	51.86	8.2	0.956	0.922	3.8
	5	64.10	60.22	6.4	1.022	0.991	3.1
0.003	7	66.73	64.40	3.6	1.042	1.023	1.9
	10	69.28	67.50	2.6	1.062	1.047	1.4
	13	71.35	69.24	3.0	1.078	1.060	1.7
	20	75.47	72.26	4.4	1.109	1.082	2.4
	2	44.34	42.03	5.5	0.850	0.833	2.1
	3	52.99	50.31	5.3	0.929	0.908	2.3
	5	60.60	57.67	5.1	0.993	0.970	2.4
0.004	7	64.61	60.91	6.1	1.026	0.996	3.0
	10	67.03	63.75	5.1	1.045	1.018	2.6
	13	69.03	66.13	4.4	1.060	1.037	2.3
	20	71.25	68.47	4.1	1.077	1.054	2.2
	2	41.56	40.43	2.8	0.823	0.817	0.7
	3	49.85	47.34	5.3	0.901	0.882	2.2
	5	56.91	53.52	6.3	0.963	0.936	2.9
0.006	7	60.63	56.63	7.1	0.994	0.962	3.3
	10	62.77	59.27	5.9	1.011	0.983	2.9
	13	64.61	60.66	6.5	1.026	0.994	3.2
	20	65.28	62.19	5.0	1.031	1.006	2.5
	2	40.30	39.00	3.3	0.810	0.803	0.9
	3	49.57	45.17	9.7	0.899	0.862	4.2
	5	55.05	50.72	8.6	0.947	0.912	3.9
0.008	7	57.04	53.14	7.3	0.964	0.932	3.4
	10	59.00	55.52	6.3	0.980	0.952	2.9
	13	59.37	56.80	4.5	0.983	0.963	2.1
	20	62.75	58.17	7.9	1.011	0.974	3.8
	2	38.83	37.98	2.2	0.795	0.793	0.3
	3	46.67	43.59	7.1	0.872	0.847	2.9
	5	51.95	48.50	7.1	0.920	0.892	3.1
0.010	7	55.30	50.81	8.8	0.949	0.912	4.0
	10	57.09	52.24	9.3	0.964	0.925	4.3
	13	58.70	53.31	10.1	0.978	0.934	4.7
	20	59.03	54.53	8.3	0.980	0.944	3.8
		average		5.0	average		2.3

https://doi.org/10.1557/jmr.2015.67 Published online by Cambridge University Press

ambiguity, methods of dual conical indentation were suggested by Chollacoop et al.[8] and Bucaille et al.[19] Without using the definition of ε_R, Swaddiwudhipong et al.[18] and Le[20] and Hyun et al.[21] found the relationship between the P–h_t curves and the material properties with sharp indentation. They then built an algorithm of reverse analysis for dual conical indentations.

At the same indentation depth, there has been misconception that conical indenter ($\theta = 70.3°$) and triangular pyramidal indenter ($\alpha = 65.3°$; Berkovich) have the same load–depth curve and projected contact area. The geometry of conical indenter has the advantage of being analytically more tractable, as well as being easier to perform in FEA. However, a significant difference between the two indenters exists for the projected contact area and contact stiffness. Shim et al.[22] showed that load–depth curves from two indenters are different due to their differences in projected contact area and contact stiffness. Similarly, Min et al.[23] have shown in FE simulations of indentation in copper that the P–h_t curve for the Berkovich indenter is a little higher than that for the 70.3° conical indenter. Therefore, an independent investigation on triangular pyramidal indentation is essential in a practical point of view.

This study focuses on the dual indentation method for property evaluation with triangular pyramidal indenters based on the reverse analysis without using the concept of representative strain. First, we check the load–depth curves of conical and triangular pyramidal indenters at the same indentation depth. FE analysis[24] is used to explore the effect of the angle of triangular pyramidal indenter on the P–h_t curve. We calculate the projected contact area, and use it for the modified equation of Young's modulus evaluation. Next, the correlation between load–depth curve and material properties is analyzed to develop an indentation property evaluation algorithm based on two triangular pyramidal indenters with different centerline-to-face angles, and to examine its validity and sensitivity.

II. COMPARISON OF PROJECTED CONTACT AREAS FOR CONICAL AND BERKOVICH INDENTATIONS

Figure 1 shows a triangular pyramidal indenter, and its equivalent axisymmetric conical indenter giving the same projected area at equal depth; Area of triangle A′B′C′ is equal to area of circle O′. The centerline-to-face angle of the triangular pyramidal indenter (α) and the corresponding half-included angle of the conical indenter (θ) are related to each other via

$$\theta = \tan^{-1}\left(\sqrt{\frac{3\sqrt{3}}{\pi}}\tan\alpha\right) \quad . \tag{3}$$

The equivalent cone angle of the Berkovich indenter ($\alpha = 65.3°$) is $\theta = 70.3°$ (Fig. 2). For the same indentation depth, we compare projected contact areas for conical and Berkovich indentations to see whether the theoretical statement is in accordance with FE results. Details on acquiring the contact area will be provided later. Figure 3 shows the finite element model for both indenters. For the FE model for conical indentation, 4-node axisymmetric elements (CAX4, Abaqus[24]) are used. Considering the symmetry of the triangular pyramidal indenter, only one sixth of indenter and specimen are modeled using three-dimensional 6-node (C3D6, Abaqus[24]) and 8-node (C3D8, Abaqus[24]) elements. The indenter is made of tungsten carbide (WC; $E_I = 537$ GPa and $\nu_I = 0.24$). We adopted the same minimum element size of FE model for conical and triangular pyramidal indentation. In simulations with WC indenters, we consider only elastic deformation of indenter. All simulations are performed to a maximum indentation depth of $h_{max} = 0.05$ mm.

The material is assumed to obey the following piecewise power law suggested by Rice and Rosengren[25]

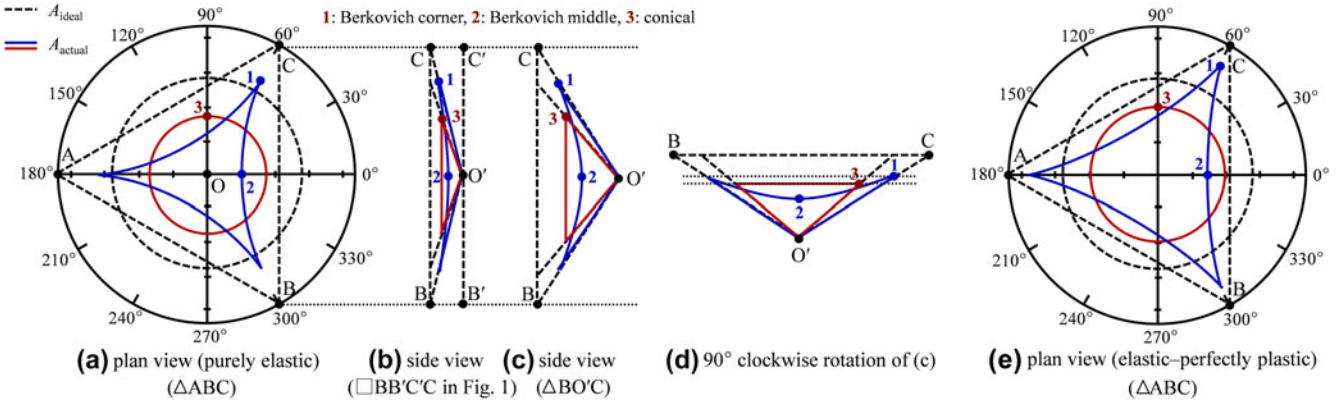


FIG. 4. The plan view and side view of indentation contact geometries in pure elastic material and elastic-perfectly-plastic material.

https://doi.org/10.1557/jmr.2015.67 Published online by Cambridge University Press

$$\frac{\varepsilon_t}{\varepsilon_0} = \begin{cases} \frac{\sigma}{\sigma_0} & \text{for } \sigma \le \sigma_0 \\ \left(\frac{\sigma}{\sigma_0}\right)^n & \text{for } \sigma > \sigma_0; 1 < n \le \infty \end{cases}, \quad (4)$$

where ε_0 ($= \sigma_0/E$) is the yield strain, E is the Young's modulus, and σ_0 is the yield strength. Total strain ε_t can be divided into elastic and plastic strain ($\varepsilon_t = \varepsilon_e + \varepsilon_p$). Hyun et al.[21] (sharp indentation) and Lee et al.[26] (spherical indentation) have shown that the influence of friction coefficient f on the load–depth curve is negligible for nonzero f. Qin et al.[27] further showed that for indenters with high indenter angles friction does not affect the load–depth curve. Since friction coefficient between metals is usually $0.1 \le f \le 0.4$, we use $f = 0.2$ in this study.

We checked the difference between projected contact areas A for 56 different materials ($E = 200$ GPa; $\varepsilon_0 = 0.001, 0.002, 0.003, 0.004, 0.006, 0.008, 0.010$; $n = 2, 3, 5, 7, 10, 13, 20$). Table I shows that the values of A obtained by Berkovich indentation are larger than the values obtained by conical indentation for all the given materials. The average gap between A values increases with increasing ε_0. Our results are consistent with the findings by Shim et al.[22] who reported that conical and Berkovich indenters produce different projected contact areas at equal indentation depths.

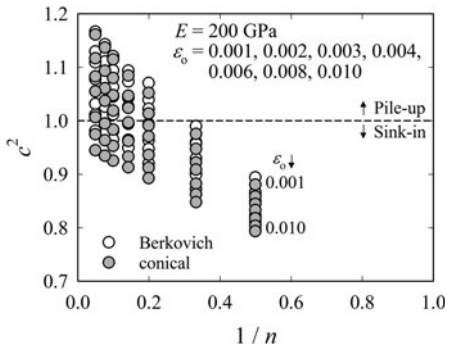


FIG. 5. Comparison of c^2 values for two different indenters.

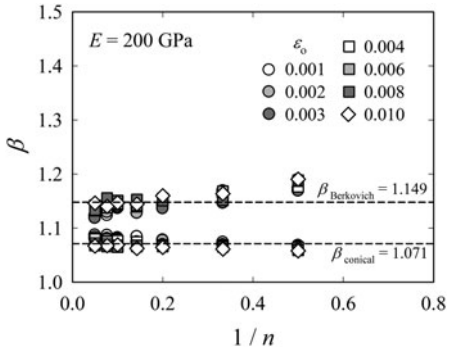


FIG. 6. β versus 1/n curves for various values of ε_0 with two different indenters.

In a fashion equal to Shim et al.,[22] Figs. 4(a) and 4(e) provide the projected contact areas at $h_{max} = 0.1$ mm for conical and Berkovich indentations of pure elastic and elastic-perfectly-plastic materials ($E = 72$ GPa, Poisson's ratio $\nu = 0.17$; $\sigma_0 = 5.5$ GPa). While for purely elastic indentation, the projected contact area for Berkovich indentation is smaller than that for conical indentation (0.094/0.099 mm^2 = 94.9%), for elastic-perfectly-plastic indentation, it is larger (0.135/0.128 mm^2 = 105.5%). Both indenters undergo sink-in for the two materials which are given. More notably, the contact line of Berkovich indenter is not in a plane differently from that of conical indenter. This is illustrated in Figs. 4(b)–4(d) which show the side views of the contact perimeters. Figure 4(b) is the contact lines projected on the rectangle BB′C′C plane of Fig. 1, and Fig. 4(c) is the contact lines for normal view to

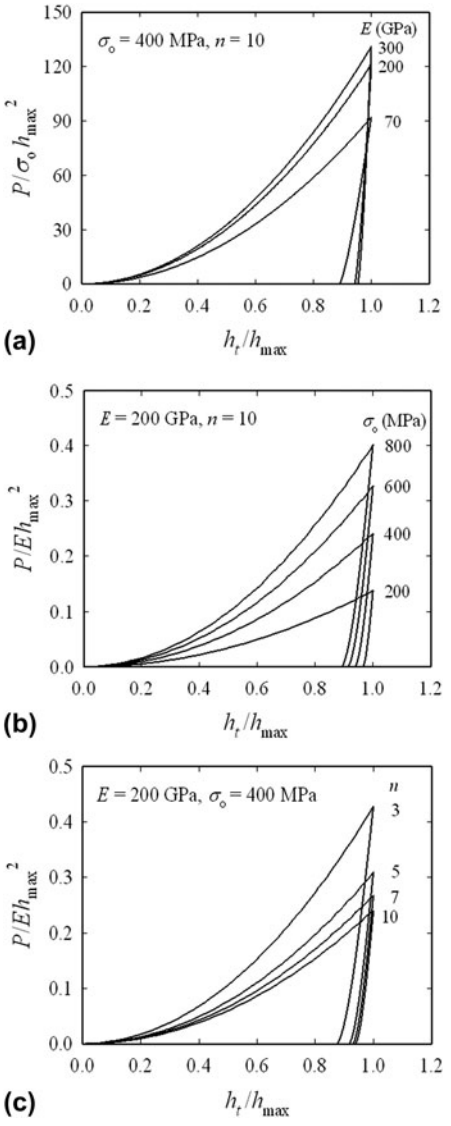


FIG. 7. Loading curves for various values of (a) Young's modulus and (b) yield strength and (c) strain hardening exponent.

https://doi.org/10.1557/jmr.2015.67 Published online by Cambridge University Press

triangle BO′C of Fig. 1. In Berkovich indentation, the concave appearance of contact impression is caused by further sink-in at the middle of indenter faces than sink-in at edges. It can readily be understood with the 90° clockwise rotation of Fig. 4(c), which results in Fig. 4(d). Nonequal projected contact areas of two indenters and nonplanar contact line of Berkovich indenter are the main sources of different indentation characteristics of two indenters.

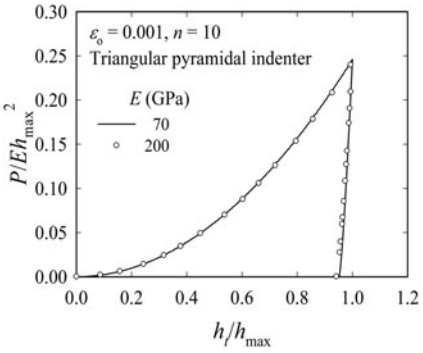


FIG. 8. Identical load–depth curves for two dissimilar materials.

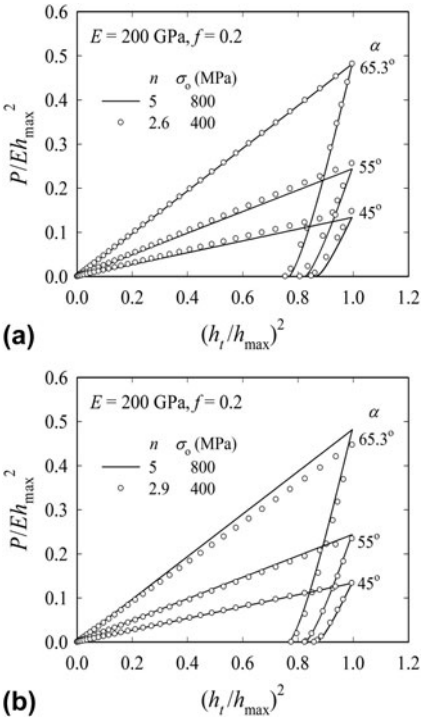


FIG. 9. Load versus depth curves for different material properties with the same C and E for (a) $\alpha = 65.3°$ and (b) $\alpha = 45°$.

To consider the pile-up/sink-in behavior we introduce the dimensionless parameters $c^2|_{conical} \equiv (h + h_g)/(h_{max} + h_g)$, $c^2_{|triangular\ pyramidal} \equiv \sqrt{A/A_t}$. Here h is the actual indentation depth considering pile-up or sink-in, and h_g is the difference between the depths obtained using conical indenters with zero and finite tip-radius.[6,21] A_t is the nominal (theoretical) projected contact area at h_{max}. In practice, it is very hard to get the projected contact area at maximum load P_{max}. The key parameter in this study is the actual projected contact area A. To evaluate the actual projected contact area A, we adopt the approach by Hay and Crawford[28] and take the intersection of the line through the last two surface nodes in contact with the line through the first two nodes not in contact (zero contact pressure) at P_{max}. For both indenters, c^2 is plotted against $1/n$ in Fig. 5. $c^2|_{triangular\ pyramidal}$ is always larger than $c^2|_{conical}$ for all elastic–plastic materials (Table I). For the evaluation of properties by a dual indentation technique, it is therefore necessary to study the triangular pyramidal indenter case separately from the conical indenter case.

III. CALCULATION OF YOUNG'S MODULUS

From the indentation P–h_t data, Young's modulus can be calculated by[29]

$$S = \beta \frac{2}{\sqrt{\pi}} E_r \sqrt{A} \quad . \tag{5}$$

Here S is the contact stiffness; E_r is the effective Young's modulus; and β is a correction factor that depends on the indenter geometry ($\beta_{Vickers} = 1.012$, $\beta_{Berk} = 1.034$).[30] The definition of E_r is

$$\frac{1}{E_r} \equiv \frac{(1-\nu^2)}{E} + \frac{(1-\nu_I^2)}{E_I} \quad . \tag{6}$$

The section regressed to get the contact stiffness S is set to $\Delta P/P_{max} = 20\%$, as in Hyun's study.[21] Hay et al.[31] considered the elastic radial displacement and proposed that β is a function of the indenter's half-included angle and Poisson's ratio. Pharr[32] derived β by assuming that the Berkovich indenter can be adequately modeled by a 70.3° cone. Similar to c^2, we check β for Berkovich and conical

TABLE II. Comparison of C values with three centerline-to-face angles.

	Kick's law coefficient C (GPa)					
α	$\sigma_0 = 800$ MPa, $n = 5.0$	$\sigma_0 = 400$ MPa, $n = 2.6$	Gap (%)	$\sigma_0 = 800$ MPa, $n = 5.0$	$\sigma_0 = 400$ MPa, $n = 2.9$	Gap (%)
45.0°	29.0	32.2	11.0	29.0	28.9	0.3
55.0°	52.2	55.1	5.3	52.2	50.2	3.8
65.3°	102.1	102.2	0.1	102.1	94.4	7.5

https://doi.org/10.1557/jmr.2015.67 Published online by Cambridge University Press

TABLE III. Material properties for FE analyses.

Material properties of indenters	α (°)	Material property	Values used in FEA
WC (E_I = 537 GPa, ν_I = 0.24)	65.3, 45.0	E (GPa)	70, 200, 300
		ν	0.3
		ε_0	0.001, 0.002, 0.003, 0.004, 0.006, 0.008, 0.01
		n	2, 3, 5, 7, 10, 13, 20

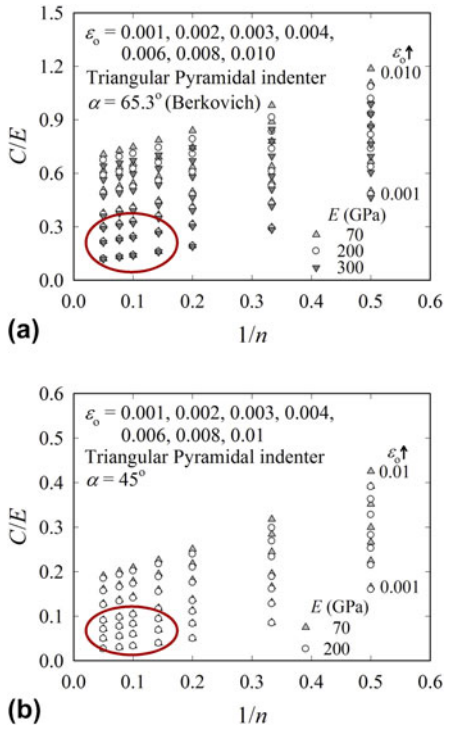


FIG. 10. C/E versus $1/n$ curves for various values of yield strain for (a) α = 65.3° and (b) α = 45°.

TABLE IV. Coefficients ψ_{ijk} of Eq. (10).

i = 1, α = 65.3°				
	k = 0	k = 1	k = 2	k = 3
j = 0	2.301×10^{-3}	1.063×10^{0}	5.330×10^{-1}	1.570×10^{-1}
j = 1	1.953×10^{-1}	1.658×10^{0}	-1.929×10^{0}	8.371×10^{-1}
j = 2	7.523×10^{-2}	3.690×10^{0}	-5.201×10^{0}	2.169×10^{0}
j = 3	1.590×10^{0}	-5.063×10^{0}	5.316×10^{0}	-1.946×10^{0}
i = 2, α = 45.0°				
	k = 0	k = 1	k = 2	k = 3
j = 0	-1.125×10^{-3}	2.241×10^{-1}	-5.825×10^{-2}	9.890×10^{-3}
j = 1	5.936×10^{-2}	6.895×10^{-1}	-7.138×10^{-1}	2.815×10^{-1}
j = 2	-9.233×10^{-2}	1.120×10^{0}	-1.363×10^{0}	5.629×10^{-1}
j = 3	7.593×10^{-1}	-1.003×10^{0}	5.980×10^{-1}	-1.126×10^{-1}

indenters for the same material properties. Figure 6 provides β values obtained for the two indenters. Since the deviation of β from its average is <5%, irrespective of material properties, β can be regarded as a constant. The average β value for Berkovich indentation (β_{Berko} = 1.149) is 6.8% higher than for conical indentation (β_{cone} = 1.071). The result is in agreement with Shim et al.[22] who found β_{Berko} = 1.141–1.158 and β_{cone} = 1.060–1.072. In this study, we take the average β_{Berko} = 1.149.

Young's modulus E can be derived by[29]

$$E = \frac{(1-\nu^2)S\sqrt{\pi}E_I}{2\beta\sqrt{A}E_I - (1-\nu_I^2)S\sqrt{\pi}} \quad . \tag{7}$$

To obtain $\sqrt{A}$ as a function of ε_0 and n we propose

$$c^2 \equiv \sqrt{A/A_t} = f^{TP}(\varepsilon_0, n) = f_{1i}^{TP}(\varepsilon_0)n^{-i} = \left(\kappa_{1ij}\,\varepsilon_0{}^j\right)n^{-i} \quad i,j = 0,1,2,3 \quad . \tag{8}$$

Inserting Eq. (8) into (7) we can write

$$E = \frac{(1-\nu^2)S\sqrt{\pi}E_I}{2\beta c^2\sqrt{A_t}E_I - (1-\nu_I^2)S\sqrt{\pi}} = \frac{(1-\nu^2)S\sqrt{\pi}E_I}{2\beta f^{TP}(\varepsilon_0, n)\sqrt{A_t}E_I - (1-\nu_I^2)S\sqrt{\pi}} \quad . \tag{9}$$

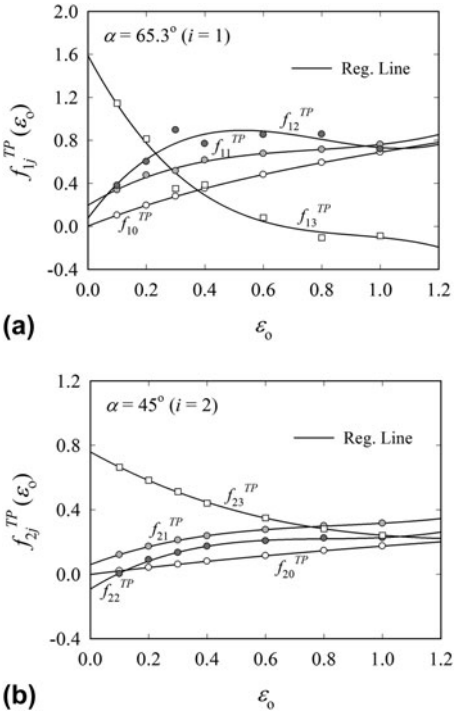


FIG. 11. Regression curves of $f_{ij}^{TP}(\varepsilon_0)$ in Eq. (9) versus ε_0 (third regression) for (a) α = 65.3° and (b) α = 45°.

https://doi.org/10.1557/jmr.2015.67 Published online by Cambridge University Press

IV. CHARACTERISTICS OF INDENTATION DEFORMATION

A. Characteristics of load–depth curves

Figure 7 shows the effects of E, σ_0, and n on the P–h_t curves for Berkovich indentation. The load P increases with E and σ_0, but decreases with n for equal h_t. Note that unloading curves vary sensitively with E. While all the material properties affect the P–h_t loading curve, the slope of unloading part is only sensitive to E. Figure 8 shows the P–h_t curve for two different materials with equal ε_0 and n. When horizontal and vertical axes are normalized by h_{max} and (Eh_{max}^2), respectively, the load–depth curves coincide, indicating the significance of ε_0 rather than the absolute values of σ_0 and E.

B. Characteristics of load–depth curves for different indenter angles

As stated above, Chen et al.[5] and Lee et al.[6] demonstrated that different materials may have equal load–depth curves and thus equal Kick's law coefficients C. Therefore, a unique stress–strain curve cannot be obtained from a single P–h_t curve. In this study, we calculate C values by regressing the data for (0.5–1) × h_{max} as Lee et al.[6] suggested. Figure 9 shows the load–depth curves of two different materials (case I: σ_0 = 800 MPa, n = 5; σ_0 = 400 MPa, n = 2.6; case II: σ_0 = 800 MPa, n = 5; σ_0 = 400 MPa, n = 2.9) with equal C and E for α = 65.3°, 55°, and 45°. While for some α, the load–depth curves coincide, they do not for other α (Fig. 9). Table II lists the gaps between C values of two materials for three α. For instance in case I, the difference between C values increases from 0 to 11% when α changes from 65.3° to 45°. This means, such two materials can be distinguished by using two self-similar indenters with different centerline-to-face angles.

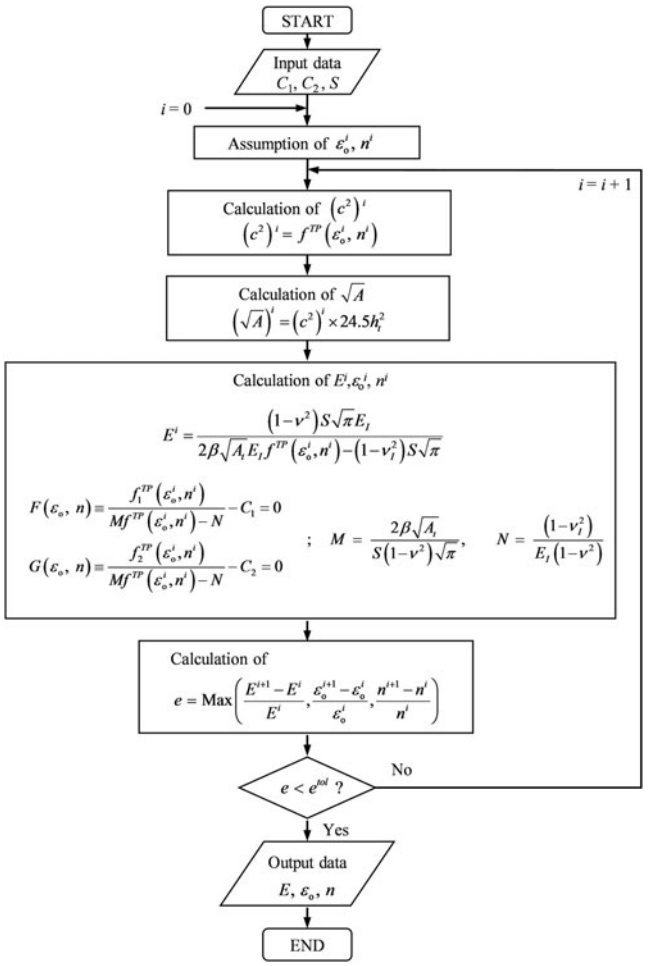


FIG. 12. Flow chart for determination of material properties.

V. NUMERICAL APPROACH BASED ON FEA SOLUTION

A. Dual indentation method for triangular pyramidal indenter

Based on the FE analysis results for a total of 294 cases (E: 3 × ε_0: 7 × n: 7 × α: 2, Table III), we propose a method for determining material properties using two triangular pyramidal indenters. In Fig. 10, C/E versus $1/n$

TABLE V. Comparison of obtained material property values to those given for E = 200 GPa.

σ_0/E ; σ_0 (MPa)	n	Obtained E	e_E (%)	Obtained σ_0	$e_{\sigma 0}$ (%)	Obtained n	e_n (%)
	2	201.6	0.8	193.5	3.2	2.0	0.4
	3	202.7	1.3	190.5	4.7	3.0	0.9
	5	201.9	0.9	193.8	3.1	4.8	4.0
0.001; 200 (MPa)	7	203.8	1.9	193.6	3.2	6.8	2.3
	10	202.5	1.2	196.4	1.8	9.8	1.6
	13	201.8	0.9	197.7	1.1	12.9	0.8
	20	202.1	1.1	194.0	3.0	19.2	4.1
	2	197.9	1.0	405.8	1.4	2.0	0.6
	3	200.1	0.0	414.1	3.5	3.0	0.9
	5	200.7	0.4	409.4	2.4	5.1	1.6
0.002; 400 (MPa)	7	200.6	0.3	411.2	2.8	7.3	3.7
	10	200.8	0.4	405.5	1.4	10.3	2.9
	13	200.9	0.4	403.7	0.9	13.4	2.7
	20	200.8	0.4	401.6	0.4	20.3	1.7
	2	196.4	1.8	618.7	3.1	2.0	0.2
	3	198.5	0.7	607.5	1.2	3.0	0.3
	5	198.9	0.5	606.8	1.1	5.0	0.8
0.003; 600 (MPa)	7	200.0	0.0	590.0	1.7	6.8	3.2
	10	199.8	0.1	601.5	0.2	10.0	0.4
	13	200.2	0.1	602.6	0.4	13.3	2.1
	20	200.4	0.2	605.1	0.9	20.9	4.3
	2	196.4	1.8	813.1	1.6	2.0	0.1
	3	197.5	1.2	796.1	0.5	3.0	0.4
	5	198.8	0.6	799.3	0.1	5.0	0.1
0.004; 800 (MPa)	7	198.8	0.6	805.0	0.6	7.1	1.3
	10	199.2	0.4	790.7	1.2	9.7	3.1
	13	200.2	0.1	796.9	0.4	12.9	0.6
	20	200.4	0.2	793.5	0.8	19.3	3.6

https://doi.org/10.1557/jmr.2015.67 Published online by Cambridge University Press

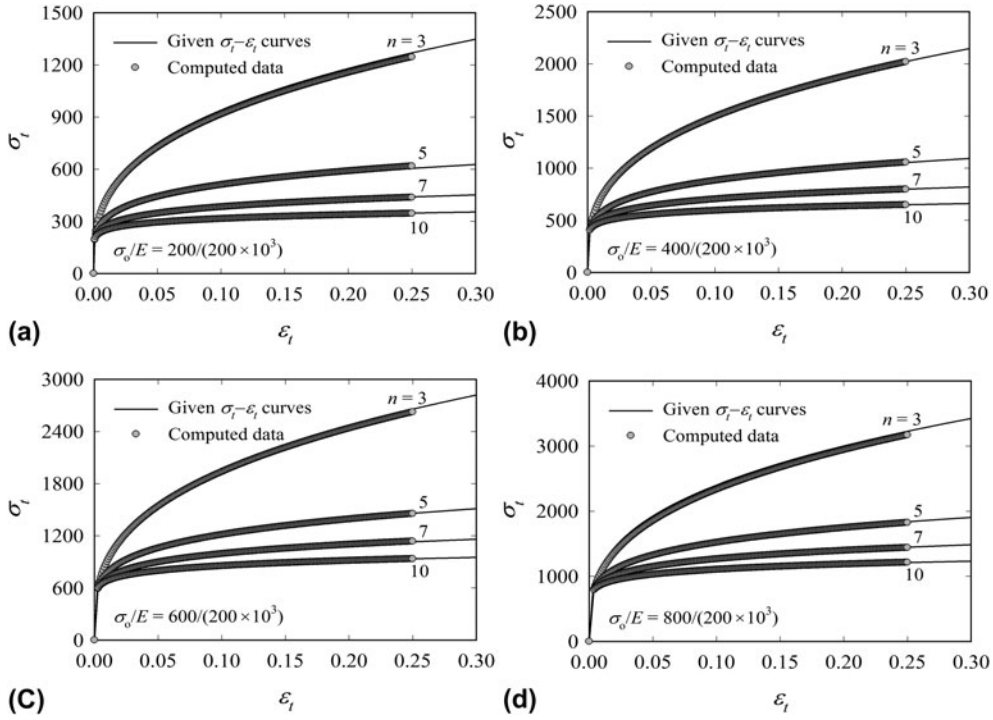


FIG. 13. Comparison of computed stress–strain curves to those given for E = 200 GPa using WC indenter [ε_0 = (a) 0.001, (b) 0.002, (c) 0.003, and (d) 0.004].

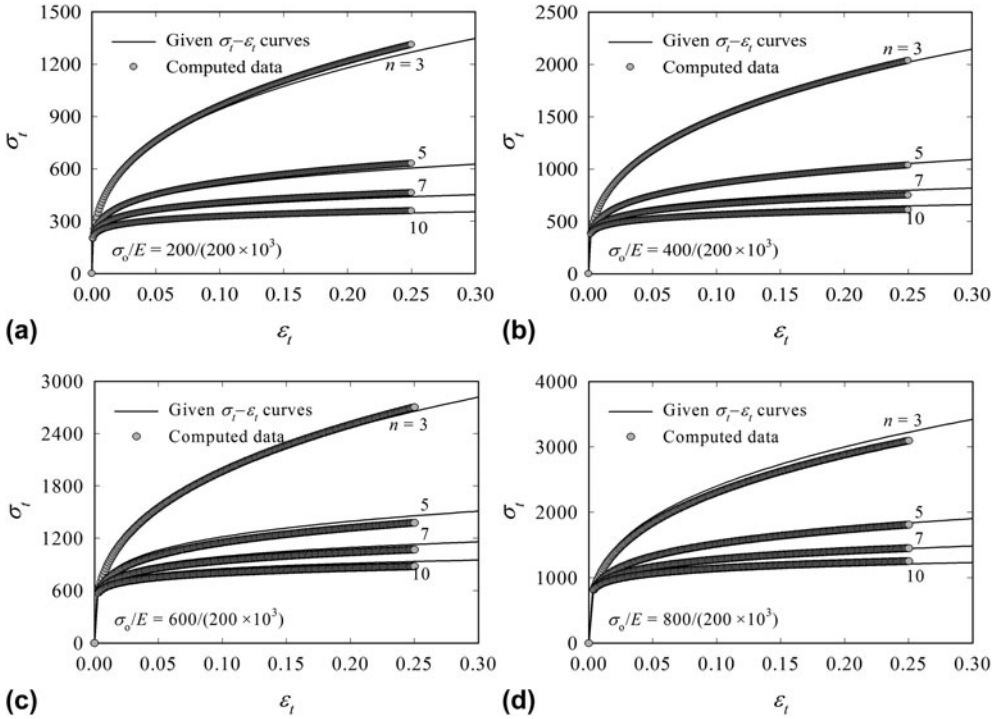


FIG. 14. Comparison of computed stress–strain curves to those given for E = 200 GPa using diamond indenter [ε_0 = (a) 0.001, (b) 0.002, (c) 0.003, and (d) 0.004].

https://doi.org/10.1557/jmr.2015.67 Published online by Cambridge University Press

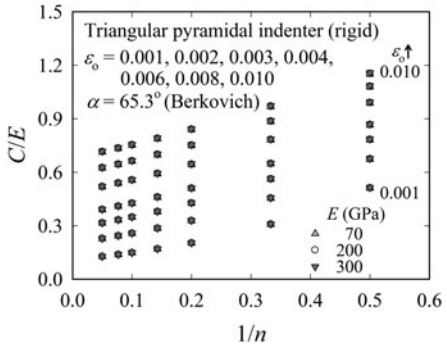


FIG. 15. C/E versus $1/n$ curves from rigid indenter for various values of yield strain.

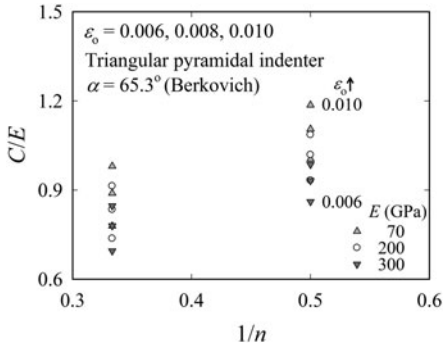


FIG. 16. Enlargement of Fig. 10(a) for the region of $\varepsilon_0 > 0.005$ and $n < 3$.

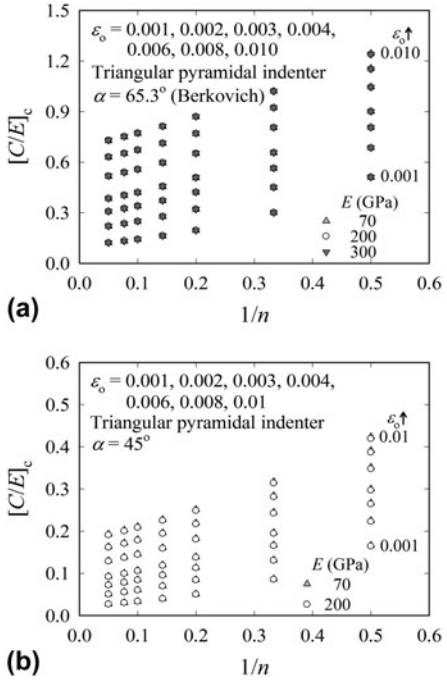


FIG. 17. $[C/E]_c$ versus $1/n$ curves for various values of yield strain for (a) $\alpha = 65.3°$ and (b) $\alpha = 45°$.

curves are shown for various values of ε_0 and $\alpha = 65.3°$ and 45°. The C values normalized by E are regressed to the following function

$$C_i/E = f_i^{\mathrm{TP}}(\varepsilon_0, n) = f_i^{\mathrm{TP}}(\varepsilon_0) n^{-j} = \left(\psi_{ijk}\, \varepsilon_0{}^k\right) n^{-j} \quad i = 1, 2\ ; \quad j, k = 0, 1, 2, 3 \quad . \tag{10}$$

The indices $i = 1$ and 2 correspond to $\alpha = 65.3°$ and 45°, respectively. The fitting coefficients ψ_{ijk} are given in Table IV. Regression curves are plotted in Fig. 11. Equation (10) is the regression equation for the material with $E = 200$ GPa.

Based on additional analysis results for $E = 70$, 200, 300 GPa and inserting Eq. (9) into Eq. (10) we can write

$$\begin{aligned} C_1 = E f_1{}^{\mathrm{TP}}(\varepsilon_0, n) &= \frac{f_1{}^{\mathrm{TP}}(\varepsilon_0, n)}{M f^{\mathrm{TP}}(\varepsilon_0, n) - N} \leftrightarrow F(\varepsilon_0, n) \\ &\equiv \frac{f_1{}^{\mathrm{TP}}(\varepsilon_0, n)}{M f^{\mathrm{TP}}(\varepsilon_0, n) - N} - C_1 = 0 \\ C_2 = E f_2{}^{\mathrm{TP}}(\varepsilon_0, n) &= \frac{f_2{}^{\mathrm{TP}}(\varepsilon_0, n)}{M f^{\mathrm{TP}}(\varepsilon_0, n) - N} \leftrightarrow G(\varepsilon_0, n) \\ &\equiv \frac{f_2{}^{\mathrm{TP}}(\varepsilon_0, n)}{M f^{\mathrm{TP}}(\varepsilon_0, n) - N} - C_2 = 0 \\ M = \frac{2\beta\sqrt{A_t}}{S(1-\nu^2)\sqrt{\pi}}, \quad N &= \frac{(1-\nu_I{}^2)}{E(1-\nu^2)} \quad . \end{aligned} \tag{11}$$

Values of ε_0 and n are determined so that $F = 0$ and $G = 0$ are satisfied. Based on Eq. (11), a program is established that extracts material properties from load–depth input data from indentations using two triangular pyramidal indenters with different α values (Fig. 12). First, C_1, C_2, and S are obtained from the P–h_t curves. Second, we assume initial values for ε_0 and n. c^2 is then calculated from Eq. (8). E is computed from Eq. (9) based on c^2 and S. We then update ε_0 and n until $F = 0$ and $G = 0$ in Eq. (11) are satisfied. E, ε_0, and n values obtained with the program are provided in Table V; the corresponding stress–strain curves are shown in Fig. 13. The average error from FE input values is about 2% for the whole range of material properties.

The program established with WC indenters ($E_I = 537$ GPa, $\nu_I = 0.24$) is also applicable for other elastic moduli, since the key variable is ε_0 (and not E or σ_0) as noted above. Inputting P–h_t data obtained with a diamond indenter ($E_I = 1000$ GPa, $\nu_I = 0.07$) into the program, and replacing the properties of WC indenter with those of diamond indenter in Eqs. (9) and (11), we obtain material properties, which are very close to those from the WC indenter (Fig. 14). The studies of Lee et al.[11,12] and Hyun et al.[21] provided a similar outcome.

https://doi.org/10.1557/jmr.2015.67 Published online by Cambridge University Press

In contrast to rigid indenters (Fig. 15), C/E obtained with elastic indenters shows some sensitivity to E (Fig. 16). Owing to the indenter deformation, C/E values become sensitive to E for $\varepsilon_0 > 0.005$ and $n < 3$. However, in engineering practice, ε_0 and n are generally <0.005 and >3, respectively (circled region of Fig. 10), so that the program based on C/E can be regarded as valid for engineering purposes. Since the values of C/E are not equal for some material property combinations, we account for the indenter deformation by introducing a correction to make the approach independent of indenter deformation. C/E and P_{max} for rigid indentation are higher than the corresponding values obtained with an elastic indenter. The approach is discussed in detail in a previous study of ours.[33] Figure 17 demonstrates that the correction yields equal C/E values independent from E.

We check the sensitivity of our approach to a change in C. We assumed an error of 2%, which is equal to the error reported by Chollacoop et al.[8] for real indentation experiments. C_1 and C_2 are simultaneously increased (or decreased) equally by 2%. The error in the estimated properties is about 3% on average (Tables VI and VII). We may therefore state that the proposed method has a rather weak sensitivity to an error in input parameters C_1 and C_2.

B. Evaluation of material properties from experimentally obtained stress–strain curves

Indentation test simulation is conducted by using the tension/compression stress–strain curve data of six actual materials from the MTS hydraulic universal material tester. Figure 18 compares the stress–strain curve from the program with the actual values. The solid line refers to the tension/compression test and the gray line is the result from the program. The predicted stress–strain curves agree well with the given stress–strain curve except for brass. For brass, yield strength from the dual indentation method is 118 MPa, far from the actual yield strength (156 MPa). In the materials disobeying the power law, the difference between the actual and estimated σ_0 is large. To estimate the properties for the materials like brass, regression functions with more variables should be used.

TABLE VI. Comparison of obtained property values (E = 200 GPa, C_1: 2% ↑, C_2: 2% ↑).

σ_0/E ; σ_0 (MPa)	n	Obtained E	e_E (%)	Obtained σ_0	$e_{\sigma 0}$ (%)	Obtained n	e_n (%)
	2	204.7	2.4	192.5	3.8	1.9	4.6
	3	204.7	2.4	190.4	4.8	2.8	6.4
	5	204.3	2.1	192.0	4.0	4.7	6.6
0.001; 200 (MPa)	7	206.4	3.2	200.2	0.1	6.7	4.0
	10	204.8	2.4	186.4	6.8	9.5	5.3
	13	203.9	1.9	189.6	5.2	11.9	8.7
	20	203.7	1.9	191.5	4.3	19.4	3.1
	2	194.0	3.0	426.7	6.7	2.0	1.6
	3	195.4	2.3	410.3	2.6	3.0	1.6
	5	196.4	1.8	400.6	0.2	5.0	0.3
0.002; 400 (MPa)	7	195.4	2.3	404.4	1.1	7.2	3.2
	10	194.9	2.6	403.4	0.8	10.3	3.2
	13	194.4	2.8	402.5	0.6	13.6	4.7
	20	194.1	3.0	399.8	0.1	19.8	0.9
	2	203.7	1.8	651.7	8.6	2.0	1.7
	3	198.8	0.6	634.0	5.7	3.0	0.9
	5	199.2	0.4	625.4	4.2	5.1	1.6
0.003; 600 (MPa)	7	200.2	0.1	610.7	1.8	6.9	2.0
	10	200.1	0.0	620.2	3.4	10.2	2.2
	13	200.5	0.2	621.4	3.6	13.6	4.4
	20	200.7	0.3	622.1	3.7	21.6	8.0
	2	196.9	1.6	860.4	7.5	2.0	0.5
	3	197.8	1.1	832.9	4.1	3.0	0.3
	5	199.1	0.5	830.2	3.8	5.1	1.6
0.004; 800 (MPa)	7	199.1	0.5	832.1	4.0	7.2	3.0
	10	199.5	0.3	817.8	2.2	9.9	0.8
	13	200.5	0.3	822.2	2.8	13.3	2.5
	20	200.7	0.4	818.9	2.4	20.2	0.9

TABLE VII. Comparison of obtained property values (E = 200 GPa, C_1: 2% ↓, C_2: 2% ↓).

σ_0/E; σ_0 (MPa)	n	Obtained E	e_E (%)	Obtained σ_0	$e_{\sigma 0}$ (%)	Obtained n	e_n (%)
	2	205.0	2.5	188.6	5.7	1.9	5.1
	3	204.6	2.3	192.4	3.8	2.8	7.2
	5	204.4	2.2	198.3	0.9	4.8	4.1
0.001; 200 (MPa)	7	206.5	3.3	188.0	6.0	6.9	1.5
	10	204.8	2.4	194.6	2.7	9.8	2.2
	13	203.9	2.0	199.8	0.1	12.6	3.1
	20	203.7	1.8	201.6	0.8	19.0	5.1
	2	197.0	1.5	376.2	5.9	2.0	1.6
	3	201.4	0.7	396.7	0.8	3.0	1.6
	5	197.4	1.3	381.0	4.8	5.0	0.3
0.002; 400 (MPa)	7	194.4	2.8	386.8	3.3	7.2	3.2
	10	195.1	2.4	390.3	2.4	10.3	3.2
	13	205.7	2.9	397.1	0.7	13.6	4.7
	20	194.7	2.7	383.5	4.1	19.8	0.9
	2	196.1	2.0	588.3	2.0	2.0	0.1
	3	198.3	0.9	584.9	2.5	3.0	0.2
	5	198.8	0.6	584.4	2.6	5.0	0.4
0.003; 600 (MPa)	7	199.8	0.1	571.5	4.8	6.7	4.4
	10	199.6	0.2	582.8	2.9	9.9	1.4
	13	199.9	0.0	585.8	2.4	13.0	0.2
	20	200.1	0.0	586.3	2.3	20.2	0.8
	2	195.9	2.0	768.1	4.0	2.0	0.2
	3	197.2	1.4	761.3	4.8	3.0	1.1
	5	198.5	0.7	770.4	3.7	4.9	1.1
0.004; 800 (MPa)	7	198.5	0.8	776.1	3.0	7.0	0.6
	10	198.9	0.6	765.6	4.3	9.5	5.3
	13	199.9	0.1	771.6	3.5	12.6	3.4
	20	200.1	0.0	770.2	3.7	18.5	7.6

https://doi.org/10.1557/jmr.2015.67 Published online by Cambridge University Press

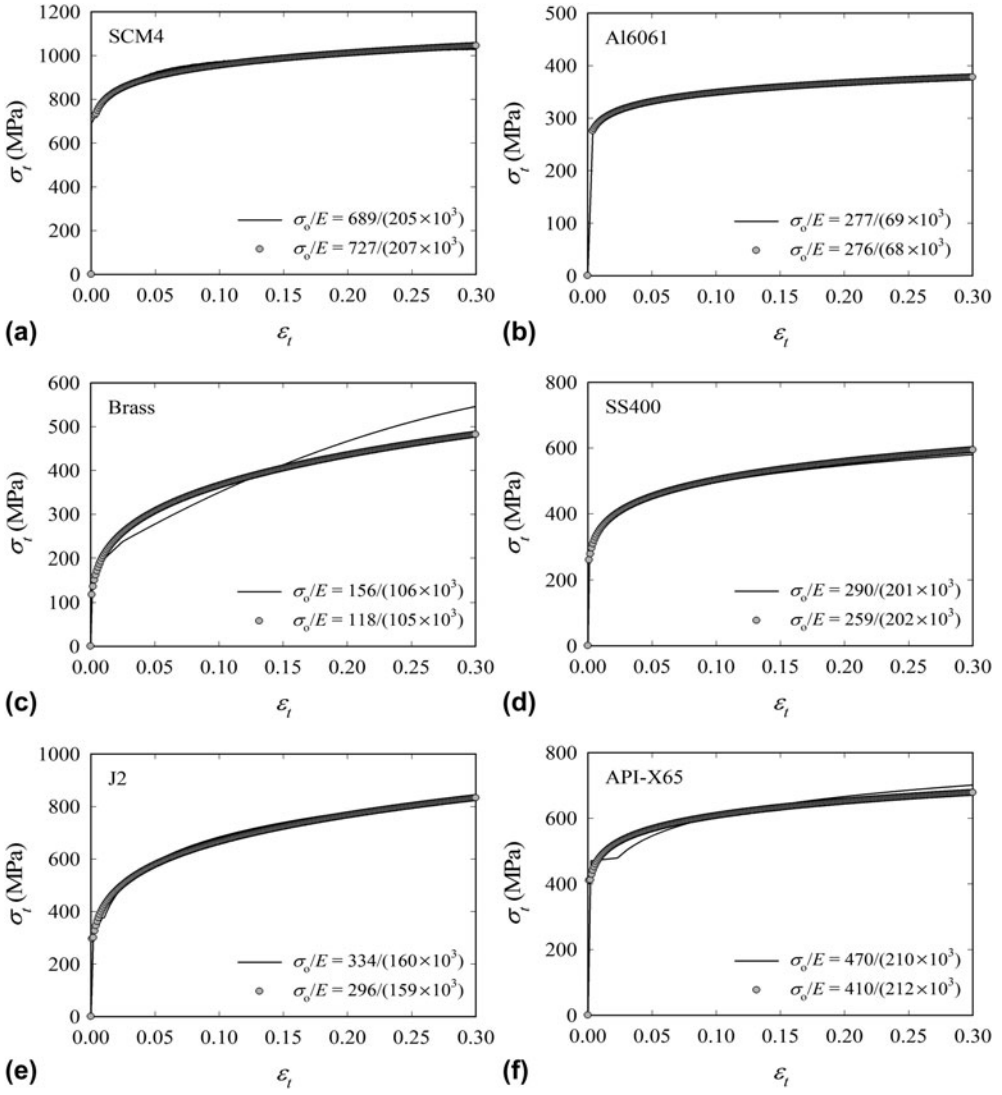


FIG. 18. Comparison between stress–strain curves computed by two parameter regression of the total strain range and those measured by experiment for (a) SCM4, (b) Al6061, (c) Brass, (d) SS400, (e) J2, and (f) API-X65.

VI. SUMMARY

Triangular pyramidal indentation has different characteristics compared to conical indentation. It is noteworthy that nonequal projected contact areas of two indenters and nonplanar contact line of Berkovich indenter are the main sources of different indentation characteristics of two indenters. We observed that two materials having the same C for a given indentation angle can be distinguished by using indenters with different indenter angles. Based on dual triangular pyramidal indentations, mapping functions were established to convert indentation load–depth to E, ε_0, and n. The proposed method holds for a wide range of material properties, with an average error $<2\%$, and shows low sensitivity to errors in the input values of C_1 and C_2.

ACKNOWLEDGMENTS

This research was supported by Basic Science Research Program through the National Research Foundation of Korea (NRF) funded by the Ministry of Science, ICT and Future Planning (No. NRF-2012 R1A2A2A 01046480).

REFERENCES

1. X. Chen, J. Yan, and A.M. Karlsson: On the determination of residual stress and mechanical properties by indentation. *Mater. Sci. Eng., A* **416**, 139–149 (2006).
2. P.L. Larsson and P. Blanchard: On the correlation between residual stresses and global indentation quantities: Numerical results for general biaxial stress fields. *Mater. Des.* **37**, 435–442 (2012).
3. J.H. Lee, D. Lim, H.C. Hyun, and H. Lee: A numerical approach to indentation technique to evaluate material properties of film-on-substrate systems. *Int. J. Solids Struct.* **49**, 1033–1043 (2012).

https://doi.org/10.1557/jmr.2015.67 Published online by Cambridge University Press

4. F. Kick: *Das Gesetz der proportionalen Widerstände und seine Anwendungen (in German)* (Felix–Verlag, Leipzig, 1885).
5. X. Chen, N. Ogasawara, M. Zhao, and N. Chiba: On the uniqueness of measuring elastoplastic properties from indentation: The indistinguishable mystical materials. *J. Mech. Phys. Solids* **55**, 1618–1660 (2007).
6. J.H. Lee, H. Lee, and D.H. Kim: A numerical approach to elastic modulus evaluation using conical indenter with finite tip radius. *J. Mater. Res.* **23**, 2528–2537 (2008).
7. M. Dao, N. Chollacoop, K.J. Van Vliet, T.A. Venkatesh, and S. Suresh: Computational modeling of the forward and reverse problems in instrumented sharp indentation. *Acta Mater.* **49**, 3899–3918 (2001).
8. N. Chollacoop, M. Dao, and S. Suresh: Depth-sensing instrumented indentation with dual sharp indenters. *Acta Mater.* **51**, 3713–3729 (2003).
9. D. Tabor: *The Hardness of Metals* (Clarendon Press, Oxford, 1951).
10. Y.P. Cao and J. Lu: A new method to extract the plastic properties of metal materials from an instrumented spherical indentation loading curve. *Acta Mater.* **52**, 4023–4032 (2004).
11. J.H. Lee, T. Kim, and H. Lee: A study on robust indentation techniques to evaluate elastic–plastic properties of metals. *Int. J. Solids. Struct.* **47**, 647–664 (2010).
12. M. Beghini, L. Bertini, and V. Fontanari: Evaluation of the stress–strain curve of metallic materials by spherical indentation. *Int. J. Solids Struct.* **43**, 2441–2459 (1994).
13. K. Bobzin, N. Bagcivan, S. Theiß, R. Brugnara, and J. Perne: Approach to determine stress strain curves by FEM supported nanoindentation. *Materialwiss. Werkstofftech.* **44**, 571–576 (2013).
14. T.F. Juliano, M.R. VanLandingham, T. Weerasooriya, and P. Moy: Extracting stress–strain and compressive yield stress information from spherical indentation. Army Res. Lab., ARL-TR-4229, 1–16 (2007).
15. J. Alkorta, J.M. Martinez-Esnaola, and J. Gil Sevillano: Absence of one-to-one correspondence between elastoplastic properties and sharp-indentation load–penetration data. *J. Mater. Res.* **20**, 432–437 (2005).
16. J. Luo, J. Lin, and T.A. Dean: A study on the determination of mechanical properties of a power-law material by its indentation force–depth curve. *Philos. Mag.* **86**, 2881–2905 (2006).
17. Y.T. Cheng and C.M. Cheng: Scaling, dimensional analysis, and indentation measurements. *Mater. Sci. Eng., R* **44**, 91–149 (2004).
18. S. Swaddiwudhipong, K.K. Tho, Z.S. Liu, and K. Zeng: Material characterization based on dual indenters. *Int. J. Solids Struct.* **42**, 69–83 (2005).
19. J.L. Bucaille, S. Stauss, E. Felder, and J. Michler: Determination of plastic properties of metals by instrumented indentation using different sharp indenters. *Acta Mater.* **51**, 1663–1678 (2003).
20. M. Le: Materials characterization by dual indenter. *Int. J. Solids Struct.* **46**, 2988–2998 (2009).
21. H.C. Hyun, M. Kim, J.H. Lee, and H. Lee: A dual conical indentation technique based on FEA solutions for property evaluation. *Mech. Mater.* **43**, 313–331 (2011).
22. S. Shim, W.C. Oliver, and G.M. Pharr: A comparison of 3d finite element simulation for Berkovich and conical indentation of fused silica. *Int. J. Surf. Sci. Eng.* **1**, 259–273 (2007).
23. L. Min, W.M. Chen, N.G. Liang, and L.D. Wang: A numerical study of indentation using indenters of different geometry. *J. Mater. Res.* **19**, 73–78 (2004).
24. Abaqus, *Abaqus User's Manual*, Version 6.12: (Dassault Systemes, Providence, RI, USA, 2012).
25. J.R. Rice and G.F. Rosengren: Plane strain deformation near a crack-tip in a power law hardening material. *J. Mech. Phys. Solids* **16**, 1–12 (1968).
26. H. Lee, J.H. Lee, and G.M. Pharr: A numerical approach to spherical indentation techniques for material property evaluation. *J. Mech. Phys. Solids* **53**, 2037–2069 (2005).
27. J. Qin, Y. Huang, K.C. Hwang, J. Song, and G.M. Pharr: The effect of indenter angle on the microindentation hardness. *Acta Mater.* **55**, 6127–6132 (2007).
28. J.L. Hay and B. Crawford: Measuring substrate-independent modulus of thin films. *J. Mater. Res.* **26**, 727–738 (2010).
29. W.C. Oliver and G.M. Pharr: An improved technique for determining hardness and elastic modulus using load and displacement sensing indentation experiments. *J. Mater. Res.* **7**, 1564–1583 (1992).
30. R.B. King: Elastic analysis of some punch problems for a layered medium. *Int. J. Solids Struct.* **23**, 1657–1664 (1987).
31. J.C. Hay, A. Bolshakov, and G.M. Pharr: A critical examination of the fundamental relations used in the analysis of nanoindentation data. *J. Mater. Res.* **14**, 2296–2305 (1999).
32. G.M. Pharr: Measurement of mechanical properties by ultra-low load indentation. *Mater. Sci. Eng., A* **253**, 151–159 (1998).
33. M. Kim, S. Bang, F. Rickhey, and H. Lee: Correction of indentation load–depth curve based on elastic deformation of sharp indenter. *Mech. Mater.* **69**, 146–158 (2014).

https://doi.org/10.1557/jmr.2015.67 Published online by Cambridge University Press